
# Highly Selective Capture of His-Labeled Enzymes on Zirconium-Based Superparamagnetic MOFS with Reliable Renewability to Improve Ph and Thermal Stability


| | |
|---|---|
| **Gaibnazarov S.B.** | Head of scientific work Doctor of Chemical Sciences |
| **Bazarov B.Kh.** | Responsible executor Director of LIQUORIGE ENGINEERING LLC |
| **ZOU DONGSHEN** | Technologist of LIQUORIGE ENGINEERING LLC |
| **Zhang Yingguo** | Technologist of LIQUORIGE ENGINEERING LLC |



**ABSTRACT**

**Organometallic frameworks** (MOFs) as a type of porous nanoparticle are promising candidates for immobilizing enzymes to increase their stability and reuse. However, most MOFSs cannot specifically immobilize enzymes and regenerate easily, which inevitably leads to serious high consumption and pollution of the environment. In this study, Renewable and magnetic MOFSs were first designed to specifically immobilize his-labeled enzymes from cell lysates without purification. Immobilized fig glucuronidase exhibited broader pH adaptability and temperature stability. The relative activity of immobilized b-glucuronidase remained at ~80% after eight cycles. It is important to note that after simple treatment, the immobilization capacity of the regenerated MOFSs, after simple treatment, was recovered by more than 90% in the first three times. Specific magnetic MOFSs have been proven to be an efficient and renewable platform for one-step immobilization and purification of His-labeled enzymes, demonstrating great potential in industrial applications of nanotechnology and biocatalysis.



**Keywords:** direct specific immobilization, His-labeled protein, renewable carrier.


## 1. Introduction

**The enzyme** is a kind of powerful biocatalyst created by nature. The rapid development of biotechnology, represented by enzymatic catalysis, has opened up new opportunities for the sustainable development of the chemical industry. an important influence on biocompatibility, biodegradability and renewability.3,4 Although the stability of enzymes has been improved by protein engineering, the sensitivity of enzymes leads to a lack of catalytic activity under extreme conditions.5,6 In addition, a large The amount of free enzymes cannot be extracted after the reaction, which remains a serious difficulty in industrial production.7, s Thus, it has been confirmed that immobilized enzymes are a useful strategy for increasing the activity, stability and selectivity of enzymes for wider application. in the biochemical and medical industry.9-12

Organometallic frameworks (MOCs) are porous carriers formed by metal ions and organic ligands through coordination bonds.13 Because of their high porosity, uniform pore size, simple modification of metal nodes and ligands, and adjustable structure and function, they have shown excellent results in a variety of applications, such as drug delivery, photonic devices, catalysis, and chemical sensing.

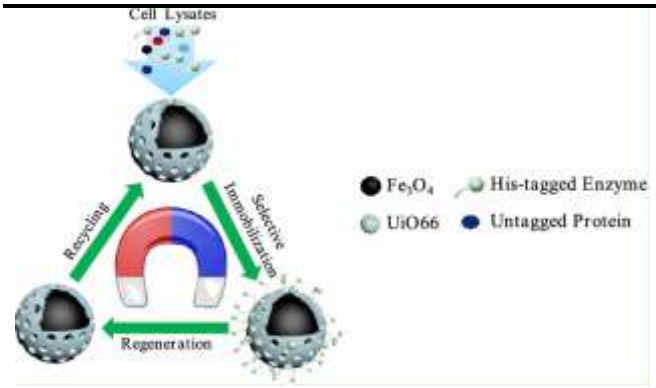


Widely used in enzyme immobilization processes due to their simple combination process and mild conditions. MOFS can protect immobilized enzymes, effectively inhibit enzyme leaching, and increase their stability under extreme conditions.1 To achieve simple separation, researchers have recently begun combining magnetic nanomaterials with MOFS, which can be easily extracted from the reaction system using an external magnet. Thus, immobilized carriers based on magnetic MOFS have attracted a lot of attention since their inception.19,20

Existing IOC immobilization techniques mainly include surface binding (physical adsorption and covalent crosslinking), infiltration (diffusion into pores or IOC cells), and co-deposition techniques.21 Although enzymes encapsulated internally retain their activity well, the combination of substrates and enzymes is limited to the mass transfer of the MOFS network. .22-24 Surface immobilization through electrostatic adsorption and hydrophobic interaction may reduce mass transfer restriction, but enzymes are more easily eliminated during the catalytic process. Covalent cross-linking solves the problem of enzyme loss, but the introduction of a cross-linking agent often inevitably leads to a loss of enzyme activity. 5, in addition, in these methods, it is necessary to use highly purified enzymes, which significantly increases the laboriousness and laboriousness of the fixation process. 26 - 28 Based on the coordination between the His-labeled protein and metal ions (Ni, Zn, Cu, Co, etc.), various materials are prepared surfacely modified with nitrilotriacetic acid or other structural analogues to achieve one-step purification and obtain immobilized enzymes. 29, 30, however, the synthesis of these specific affinity materials often requires sophisticated techniques that limit the large-scale production of immobilized enzymes. As a kind of carrier formed by metal ions and organic ligands, MOFS has many regions of unsaturation that can form coordination with His-labeled proteins. However, several studies have reported specific immobilization of magnetic MOFS. 31 Meanwhile, if not handled properly, heavy metals and organic ligands can lead to new and serious environmental pollution.

In this study, magnetic and renewable Zr-based MOFS (Fe3O4@UiO66) were synthesized for the first time for highly selective immobilization of His-labeled enzymes by coordinating surface unsaturated Zr 4+ and histidine (Scheme 1). For the medically important glucuronic hydrolase, His-labeled in -glucuronidase was chosen as the model system. We proved that the prepared magnetic MOFS can directly immobilize the target protein from cell lysates with a high immobilization coefficient. Immobilized β-glucuronidase showed significant improvement in alkaline environments, high temperature, protease degradation and restriction of by-products. The immobilized enzymes retained high catalytic activity after repeated reuse. It is important to note that Zr-based magnetic MOFS can be regenerated after simple processing with a good immobilization factor after several cycles.

## Materials And Methods

### Reagents and materials.

The genes in glucuronidase and primers used in this study were acquired from Sangon Biotech (Shanghai). Escherichia coli trans5a and BL21 (DE3) were obtained from TransGene Biotech (Beijing). FeCl3·6H2O, FeCl2·4H2O, ZrCf^1,4-dicarboxybenzene (TPA) and GL were purchased from Macklin (Shanghai). The GA (99%), glycyrrhetinic acid glucuronide (GAMG 99%) and GL (99%) standards were obtained from Shanghai Yuanye Bio-Technology Co. Ltd. All other reagents used in this experiment were analytically pure.

**Expression and purification in-glucuronidase.**

We screened for aspergillus bertholletiae with NCBI (KAE8374379.1) and named it AbGUS. For the design of the recombinant plasmid, pET28a (+) was chosen (Fig. S1A ), and the expression of recombinase was in E. coli BL21 (DE3). Purification in-glucuronidase was carried out by Ni-chelated affinity chromatography. 32 Process details shown on

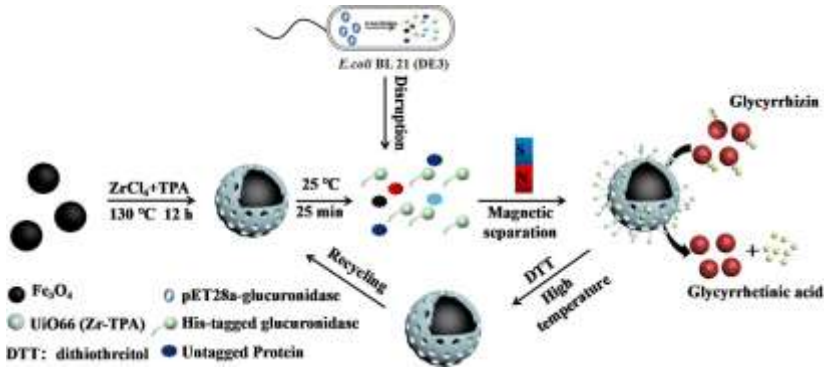


Figure 1. Production of magnetic MOFs based on Zr(lV) and selective capture of His-labeled enzymes

Nanoparticles $Fe_3O_4$. The method of co-precipitation with some modifications was used to obtain nanoparticles Fe3O4. 33 First, 2 g of FeC^^^O (2 g), 8 g of NaAc and 2 g of PEG 4000 were added to 80 ml of ethylene glycol when stirred. Then all mixtures were transferred to an autoclave of stainless steel with a Teflon coating and kept at 200 ° C for 8 hours. $Fe_3O_4$ nanoparticles three times purified with ethanol and deionized water. The $Fe_3O_4$ nanoparticles were then dried in a furnace at 60° C. for 8 hours and assembled for later use.

**UiO66 based on Zr(IV), applied to Fe3O4** nanoparticles**.**

The prepared $Fe_3O_4$ nanoparticles (100 mg) were dispersed in dimethylformamide (DMFA) (5 ml) and sonicated for 30 min. Then 150 mg ZrCl 4, 130 mg terephthalic acid, 75 ml DMFA and 4 ml of glacial acetic acid were added. The mixture was then transferred to a Teflon-coated stainless steel autoclave and reacted at 130 °C for 10 hours. Next, the brown precipitate was separated with a magnet and washed three times with ethanol and deionized water for removal of impurities. The resulting $Fe_3O_4$@UiO66 was dispersed in deionized water for subsequent experiments.

**Специфическая иммобилизация AbGUS $Fe_3O_4$@UiO 66.**

The immobilized enzyme was prepared according to preferences with a slight modification. 34 AbGUS and bovine serum albumin (BSA) (0.8 mg/ml) in phosphate buffer (PB, pH 7.4, 20 mM) were mixed together with nearly 3 mg $Fe_3O_4$ and $Fe_3O_4$@UiO66 respectively. The mixtures were then shaken at 25° C. and 800 rpm for 30 min. After the reaction was completed, electrophoresis was performed in a polyacrylamide gel with sodium dodecyl sulfate (SDS-PAGE) to test the adsorption specificity. Determination of the coefficient loading was based on the Bradford method of the amount of protein after immobilization

$$\text{Load Factor} = \frac{\text{amount of protein after immobilization}}{\text{total amount of protein for immobilization}}$$

**Analysis of enzymatic activity.**

For further determination of the hydrolysis activity of free and immobilized AbGUS, 1 mg/ml of glycyrrhizic acid (GL) in FB (pH 5.0, 20 mM) was prepared. Free enzymes (40 μL, 0.1 mg/mL) and immobilized enzymes (containing 0.004 mg AbGUS) were added respectively to 1 mL of AP solution. The reaction

was incubated at 40° C. and 220 rpm for 15 min. 800 µL of methanol was then added to stop the reaction. The resulting glycyrrhetinic acid (HA) was determined by high-performance liquid chromatography (HPLC) after filtration through an organic microporous membrane of 0.22 µm. The Shimadzu LC-15C system was equipped with a Diamonsil C^ (4.6×250 mm 2, 5 µm) speaker. The mobile phase was methanol (95%) and water (5%) at a flow rate of 0.8 ml / min. UV detection was carried out at 250 nm for GL and GA.

**Analysis of the stability of free and immobilized AbGUS.**

Stability at different temperatures was determined through the relative activity of free and immobilized AbGUS stored in FB (20 mM) with a pH of 5.0 in the temperature range from 25 to 70 ° C for 2 h. Similarly, pH stability was incubated in PB at 25 ° C with a pH range of 3.0 to 9.0 for 2 hours. Long-term storage stability was determined by storing free and immobilized AbGUS in 20 mM pH 5.0 PB at 4 °C for 7 days. For the hydrolysis of the AP, the same amount of free and immobilized enzymes was taken daily. The effect of glucuronic acid concentration on catalytic activity was measured in the range from 1 to 8m.

Under the above conditions, the number of cycles of immobilized enzymes was measured and 1 ml of 1 mg / ml of GL solution with immobilized enzymes was incubated for 15 min. After that, the immobilized enzymes were separated with a magnet, and the precipitate was washed three times with 1 ml of FB (pH 5.0, 20 mM) to remove HA and unreacted GL for reuse in the next cycle.

Relative activity was calculated according to the following equation (equation 2)

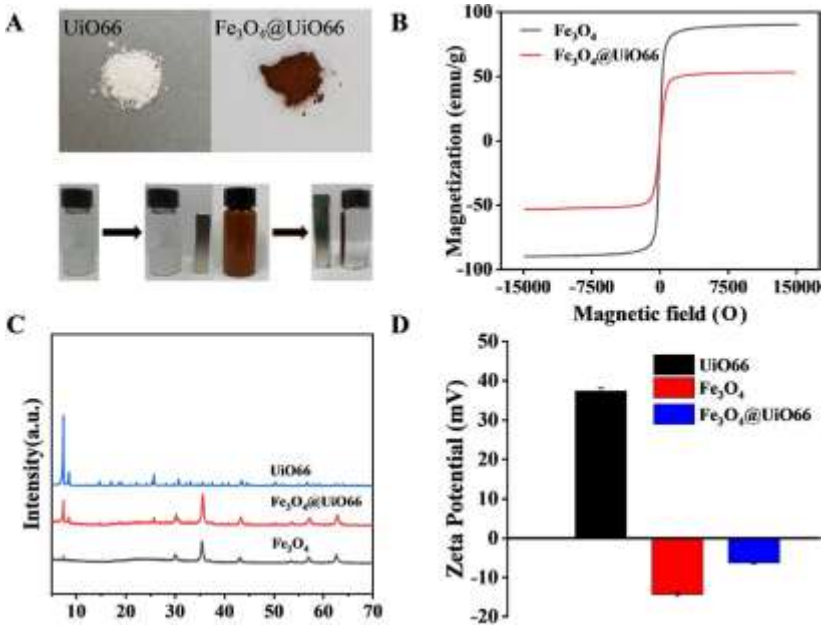


**Рис. 1. Физические свойства $Fe_3O_4$@UiO66: (A) синтезированные UiO66 и $Fe_3O_4$@UiO66. (B) VSM $Fe_3O_4$ (черный) и $Fe_3O_4$@UiO66 (красный) при 1,5 Тл. (C) XRD UiO66 (синий), $Fe_3O_4$ (черный) и $Fe_3O_4$@UiO66 (красный) при 1,5 Тл. (C) XRD UiO66 (синий), $Fe_3O_4$ (черный) и $Fe_3O_4$@UiO66 (красный). (D) f-потенциалы UiO66, $Fe_3O_4$ и $Fe_3O_4$@UiO66.**

$$\text{relative activity} = \frac{A_0}{Ax}$$

And$_0$ is the highest activity of one group.

Ax are the ones that others have.

Characteristics. To confirm the Zr-based coating of Zr-based MOFS UiO66 around the surface of Fe3O4 nanoparticles, to observe the morphology and microstructure of the samples. To characterize the functional groups, fourier transform infrared spectroscopy was

performed (FTIR, Nicolet spectrometer model 205). A vibrating magnetometer for samples (VSM, Quantum Design) was used to determine the magnetic properties of samples at 25 °C with a magnetic field ranging from -15 up to 15 kOe. Determinations of thermogravimetric (TG) analysis were performed on the thermogravimetric analyzer STA 449 to determine the stability of $Fe_3O_4$@UiO66. X-ray diffraction analysis (XRD, Rigaku) $Fe_3O_4$@UiO66 was performed on an X-ray diffractometer D8 advance with Cu Ka-radiation ( λ = 1.5406 nm, 40 kV x 40 mA). The porous structure was studied by Brunauer-Emmet-Teller (BET) and Barrett-Joyner-Halenda (BJH). Confocal laser scanning microscopy (CLSM, LEICA TCS SP8) was used for visual observation of immobilized enzymes. f-Potential was tested on Zeta/sizer Nano 9300 instruments to determine potential changes after UiO66 coverage.

## Results And Discussion

### Синтез и характеристика $Fe_3O_4$ @UiO66.

The introduction of a magnetic core is a possible method of improving the recovery of MOFS nanomaterials. Here, the Fe3O4 nanoparticles were chosen as the magnetic core coated with Zr-based MOFS UiO66. Like the Fe3O4 nanoparticles, the resulting materials Fe3O4@UiO66 looked like brown precipitates, while the Zr(IV)-based IOC UiO66 without magnetic nanoparticles were white solid particles (Fig. 1A). In Figure 1B, the saturation magnetization value of **$Fe_3O_4$@UiO66** is 53.09 emu/g, and the value of **the $Fe_3O_4$** nanoparticles is 90.02 eme/g. The change in magnetic response also indicated the formation of the core-shell structure. The resulting **$Fe_3O_4$@UiO66** it can still be easily separated by an external magnet, while UiO66 has no magnetic response (Fig. 1A). Thus, the resulting hybrid nanoparticles have a good magnetic separation property, which has great potential for practical applications.

The fabrication of the Fe3O4@UiO66 was further characterized using XRD (Fig. 1 C). Figure UiO66 (20 = 7.36, 8.52 and 25.7°) corresponded to the planes (110), (200) and (600), which is well consistent with previous studies, indicating the growth of the UiO66 crystal on the surface **of $Fe_3O_4$**. 35 In addition, the main diffraction peaks **of $Fe_3O_4$** are found in Fe 3 3 nanocomposites. **$O_4$@UiO66**. Characteristic peaks at 30.1, 35.4 and 43.2° correspond to the planes (220), (311) and (400) of the cubic crystal system. The graphs showed that the nanocomposites Fe3O4@UiO66 include both the characteristic peaks of the fe 3 O 4 core nanoparticles and the mofs uiO66 shell, 36 confirming the formation of the **$Fe_3$** O core shell **$_4$@UiO66**. In the PBS buffer (pH 7.4), the Z potential of the UiO66 nanoparticles was +37.3 mV, and **$fe_3O$** 4-14.3 mV (Fig. 1D). After wrapping the IOC UiO66, the potential of the magnetic nanoparticles changed to -6 mV. The coating of fe **$_3O_4$** moF s nanoparticles based on Zr was maintained.

EMS and TEM were used to further confirm the formation of MOFS UiO66 based on Zr around the surface **of $Fe_3O_4$**. From

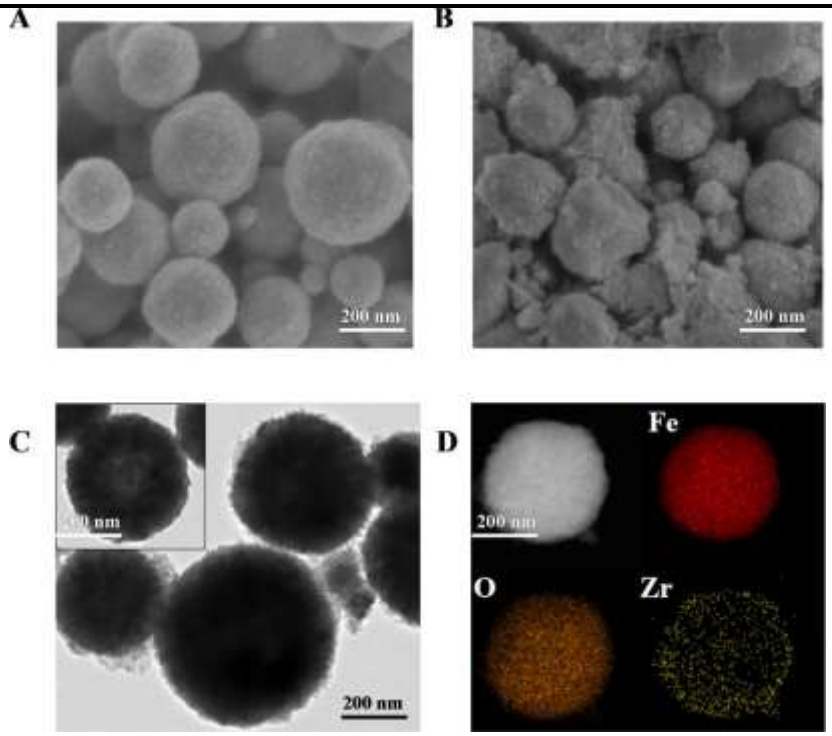


**Рис. 2. Морфология и микроструктура $Fe_3O_4$ и Fe3O4@UiO66, распределение элементов на $Fe_3O_4$@UiO66: СЭМ $Fe_3O_4$ (A) и $Fe_3O_4$@UiO66 (B). (C) ПЭМ $Fe_3O_4$ (вставленное фото в (C)) и $Fe_3O_4$@UiO66. (D) распределение элементов, показанное ПЭМ-картированием $Fe_3O_4$@UiO66. Масштабная линейка: 200 нм.**

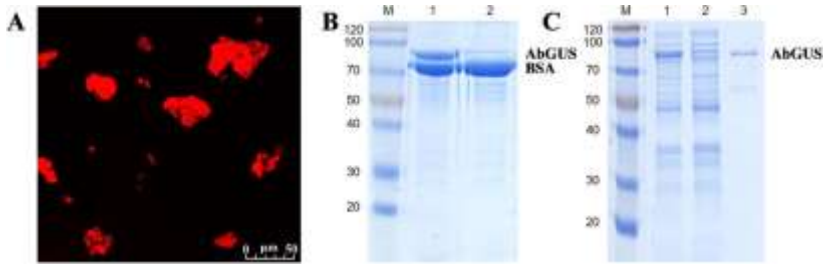


**Figure 3. (A) Micrograph of confocal fluorescence $Fe_3O_4$@UiO66@AbGUS. (B) SDS-PAGE products before (track 1) and after (track 2) immobilization on $Fe_3O_4$@UiO66. (C) SDS-PAGE cell lysates before (track 1) and after immobilization with $Fe_3O_4$@UiO66 (track 2) and uncovered $Fe_3O_4$ (track 3).**

The EMS image in Fig. 2A shows that the $Fe_3O_4$ nanoparticles have a spherical or ellipsoidal shape and a smooth surface. When UiO66 was coated, the surface of the samples became rough and uneven (Fig. 2B), which increased the surface area of the BET carriers and provided more adhesion sites and a good microenvironment for enzymes. Unlike the $Fe_3O_4$ nanospheres. (inserted photo on Fig. 2 C), $Fe_3O_4$@UiO66 demonstrates a kernel-shell structure with a thin and loose shell UiO66. TEM $Fe_3O_4$@UiO66 had a darker electron density, which further supported the surface coating. We also characterized

pdistribution of elements on $Fe_3O_4$@ UiO66. As shown in Figure 2D, zirconium was distributed along the periphery of the magnetic nanoparticle, confirming that Zr-based UiO66 was deposited on the surface of Fe3O4. Compared to the elements Fe and O, the density of zirconium elements was relatively less. The UiO66 layer could be loosely distributed on the surface of the Fe3O4 nanoparticles. , which explains why the Z-potential of Fe3O4@UiO66 was not positive like that of UiO66.

**Специфическая иммобилизация His-меченых ферментов на $Fe_3O_4$@UiO66.**

Next, we investigated the specific immobilization of His-labeled AbGUS with $Fe_3O_4$@UiO66. We then used CLSM to visually observe the immobilized enzymes. For this, the purified recombinant AbGUS was labeled with rhodamine B (RhB). 37 The released red fluorescence of RhB radiation confirmed the presence of AbGUS in hybrid fe $_3O_4$ nanocomposites@UiO66 (Fig. 3 A). To confirm the high selectivity of $Fe_3O_4$@UiO66, we first prepared a mixed solution of BSA and His-labeled AbGUS with a protein concentration of 0.8 mg/ml. As shown in Track 1 in Fig. 3B, the protein solution prior to immobilization showed two dark blue bands at 80 and 66.4 kDa per SDS-PAGE, corresponding to AbGUS and BSA, respectively. After mixing with Fe3O4@UiO66 and separation by means of an external magnet, the strip for AbGUS in the protein mixture became much lighter (track 2 in Fig. 3B). In contrast, the BSA strip was still heavy, indicating that the BSA could not be captured Fe3O4@UiO66.

the use of cell lysates Fe3O4@UiO66 demonstrated higher selectivity in capturing His-labeled AbGUS, whereas the bands of unlabeled protein on track 2 remained unchanged compared to the strip on track 1 in Figure 3C. However, uncoated Fe3O4 nanoparticles absorbed all proteins, including the unlabeled protein (track 3 of Figure 3C). As shown in Figure S2, the surface of the Fe3O4@UiO66@AbGUS has a coarse morphology. The result of EMS and FEM showed no obvious changes Fe3O4@UiO66 before and after enzyme immobilization, which is similar to previous studies. 36, 38 We then measure the magnetic nanoparticles loaded with enzymes. Since the charge of the enzyme was negative, the surface potential changed from -6.23 to -21.21 mV, which indicates a successful loading enzymes on the Fe3O4@UiO66.

To further confirm that the strong interaction of the His-label with Zr(IV) leads to high immobilization of the target protein, we tested the change in the adsorption capacity of Fe3O4@ UiO66 to His-labeled AbGUS at different concentrations of imidazole. As shown in Figure S3, when the concentration of imidazole was 500 mM, the protein was not adsorbed. A small portion of the target protein was immobilized at 200 mM imidazole. Almost all His-labeled AbGUS were absorbed without imidazole in solution. Thus, due to the strong competition of imidazole, the His label cannot effectively bind to Zr(IV). However, the concentration of unlabeled protein remained unchanged regardless of the presence of imidazole. All of the above results showed that $Fe_3O_4$@UiO66 does achieve specific adsorption due to the interaction between the surface unsaturated Zr(IV) and the histidine imidazole ring in the His-labeled protein. The immobilized His-labeled AbGUS with $Fe_3O_4$@UiO66 was named $Fe_3O_4$@UiO66 @AbGUS.

To better prove the immobilization of $Fe_3O_4$@UiO66 and AbGUS labeled By His, an FTIR was conducted to characterize functional groups. As shown in Fig. 4A, the characteristic peaks of 1560 and 1402 cm-1 refer to the oscillation of -COOH on UiO66, and the peaks of 746 and 626 cm -1 refer to the oscillation of Zr-O, indicating the formation of

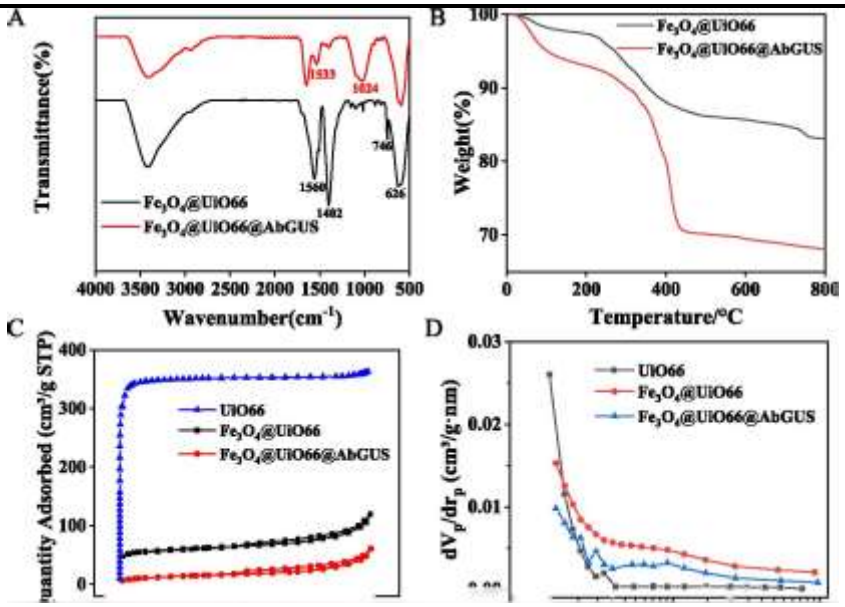


**Rice. 4. (A) FTIR of 500 to 4000 cm-1 of free and immobilized enzymes and (B) TG of synthesized nanocomposites. Size distribution of BJH pores (C) and nitrogen adsorption/desorption isotherms (D) UiO66, Fe3O4@UiO66 and Fe3O4@UiO66@AbGUS.**

The UiO66 coating on $Fe_3O_4$. The absorption peak originally belonging to Fe-O can be affected by Zr-O, resulting in the overlap of two absorption peaks. After immobilization, the peak of $Fe_3O_4$@UiO66@AbGUS showed new adsorption bands at 1533 cm -1, which was the deformation oscillation of the NH 2 groups from AbGUS. The cn tensile vibration formed a characteristic peak at 1024 cm -1. In fact, the FTIR spectrum is also indicative of the immobilization of AbGUS on composites.

The thermal stability of $Fe_3O_4$@UiO66@AbGUS in the range from 25 to 800 °C (Fig. 4 B) was studied using TG analysis. Mass loss up to 220 °C was caused by the release of solvent molecules adsorbed in the cavity $Fe_3O_4$@UiO66. The corresponding mass loss at 220° C. was the conversion of $Fe_3O_4$ to y-$Fe_2O_3$. y-$Fe_2O_3$ was then converted to a-$Fe_2O_3$ at 400 °C, 40 with an overall weight loss of 10%. Total weight loss Fe3O4@UiO66 was only 17% at 800 °C, indicating high thermal stability. For comparison, $Fe_3O_4$@UiO66@AbGUS showed a mass loss of ~18.7% in the range of 220-400 °C, which confirms the immobilization of AbGUS on $Fe_3O_4$@UiO66. Judging by the changes in the quality of AbGUS and $Fe_3O_4$@UiO66, the enzyme load was 230 mg / g of carrier.

BETH and DBX methods are widely used to study the adsorption properties of particles. Adsorption/desorption of nitrogen was carried out on UiO66, $Fe_3O_4$@UiO66 and $Fe_3O_4$@UiO66@AbGUS. The corresponding isotherms are shown in Figure 4 C. According to the previous report, 36 Fe3O4has a type II adsorption isotherm. The UiO66 adsorption/desorption isotherm is type I, while $Fe_3O_4$@UiO66 and $Fe_3O_4$@UiO66@AbGUS must exhibit a mixture of type I/II isotherms. As shown in Table 1, the beet surface area of Fe3O4particles clearly increased from 38.1 to 193.6 m2 / g after applying UiO66 to it. 33 Similarly, the pore volume increased from 0.014 to 0.113 cm3 / g. The pore size distribution of the nanoparticles was analyzed using BJH, and the results are shown in Figure 4D. The micromesoporous structure of UiO66 provides a large surface area for magnetic fields.

Table 1. BET surface area and pore volumes of the obtained magnetic materials

| Samples | BAT surface area ($m^2$/g) | pore volume ($cm^3$/g) |
|---|---|---|
| $Fe_5O_4$ 33 | 38.1 | |
| UiO66 | 1427.24 | 0.531 |

| | | |
|---|---|---|
| Fe3O4@UiO66 | 193.6 | 0.113 |
| Fe3O4@UiO66@AbGUS | 47.372 | 0,088 |

nanoparticles. Moreover, $Fe_3O_4$@UiO66 has a larger pore size of about 10 nm than UiO66, which allows the enzymes in the POres of MOFS to be immobilized through coordination. The porous structure also allows the substrate to diffuse more easily. After absorbing His-labeled AbGUS, the specific surface area of the BET and the pore volume of hybrid composites decreased by 75% and 22%, respectively (Table 1). Thus, His-labeled AbGUS not only adsorbed on the surface of hybrid nanoparticles, but also diffused into the pores of MOFS.

**Optimal working conditions of free and immobilized enzymes.**

Immobilized enzymes. According to the above results, $Fe_3O_4$@UiO66 can effectively and specifically immobilize His-labeled AbGUS from cellular lysates. Next, we analyzed the recovery of enzymatic activity by one-step purification and immobilization (Fig. 5A). As one of the main active ingredients in licorice, GL can be hydrolyzed by AbGUS to form GA. As the number of carriers increased, the protein content of the supernatant gradually decreased (Fig. S4). When the carriers reached a concentration of 8 mg/ml, 94% of the enzymatic activity of AbGUS was recovered from cellular lysates. Through simple mixing and separation with magnetic nanomaterials, recombinant AbGUS can be perfectly extracted from cell lysates, demonstrating great potential for practical applications.

The capacity and efficiency of immobilized enzymes play a significant role in the practical application of biocatalysis. First, we optimized the media load factor and immobilization time using the cleaned AbGUS. With the use of 3 mg of $Fe_3O_4$@ UiO66 nanoparticles, protein loading increased with increasing protein concentration, and the highest loading factor reached 84.49% at 0.8 mg/ml AbGUS (Fig. S5). The enzyme load per carrier unit could be 225.3 mg/g of carrier, which was consistent with the TG results. In addition, the $Fe_3O_4$@UiO66 nanoparticles could completely capture His-based on this immobilization time. Compared to other magnetic MOFS, the 21' 25' 41 $Fe_3O_4$@UiO66 obtained in this experiment had a higher loading capacity and load factor, which significantly reduced carrier waste and protein loss in practice. Applications.

The action of immobilized AbGUS with different pH values was tested in the pH range from 3.0 to 7.0 (Figure 5A). The optimal pH of free and immobilized AbGUS was 5.0, but $Fe_3O_4$@UiO66@AbGUS had a wider pH range and maintained a higher activity from pH 4.0 to 6.0. The activity of $Fe_3O_4$@UiO66@AbGUS at pH 4.5 and 5.5 was 86.9 and 73.6%, respectively. The effect of temperature for free and immobilized AbGUS on the catalysis reaction from 25 to 75 ° C was analyzed. Shown in Figure 5B, the maximum activity of $Fe_3O_4$@UiO66@AbGUS was at 50 ° C, while the activity of free enzymes was at 40 ° C. Moreover, the immobilized AbGUS showed better heat resistance at temperatures above 60 ° C. Ensuring optimal reaction conditions was due to the protection of the active sites and the conformation of enzymes by immobilization on $Fe_3O_4$@UiO66 .

The kinetic parameters of free and immobilized enzymes were studied by measuring the hydrolysis of the AP with different substrate concentrations at optimal pH and temperature values. In Table. The 2 V max of immobilized AbGUS (1.8023 ± 0.136 μM/s) is slightly reduced compared to free enzymes (2.079 ± 0.226 μM/s). This phenomenon may explain the lower availability of GL and the change in local charge near the active site of the enzymes. 42 The value of K m $Fe_3O_4$@UiO66@AbGUS increased by about 28% compared to free enzymes. The value of k cat /K m of immobilized enzymes decreased by 41.8%. The reason for the increase in Km may be the diffusion limitation of substrates near $Fe_3O_4$@UiO66 @ AbGUS and/or local conformational change of the active site of enzymes. 43, 44 Even if immobilization reduces the flexibility of enzymes, immobilized AbGUS will still surpass it in stability, reuseability, and potential efficacy. Excellent stability of $Fe_3O_4$@UiO66@AbGUS: acid, alkali, long-term storage and cycles. Unlike

free enzymes, one of the main advantages of immobilized enzymes was that they could improve the tolerance of enzymes under harsh conditions such as high temperatures, acids and alkalis. 45-47 The stability of $Fe_3O_4$@UiO66@AbGUS was.

Figure 5. (A) Scheme for converting GL to GA $Fe_3O_4$@UiO66@AbGUS. Optimization of hydrolysis conditions: relative activity at different pH (B) and temperature (C).

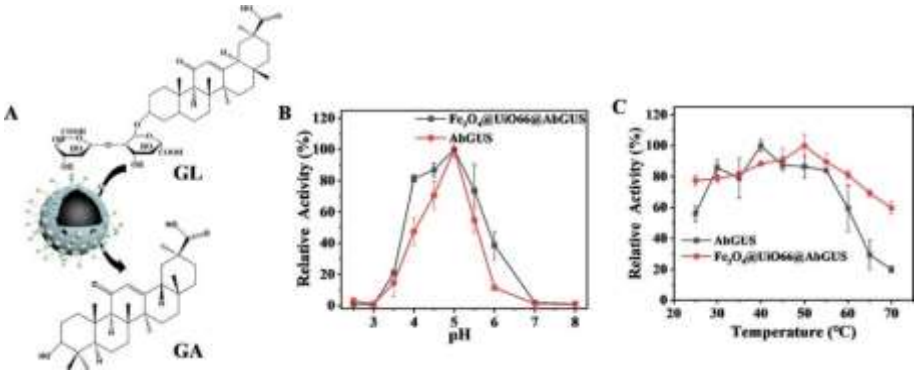


Table 2. Kinetic parameters of free and immobilization enzymes.

| | Vmax ($_{UM-S-1}$) | Km (mM) | $^{k}$cat ($_{S-1}$) | fccat/Km |
|---|---|---|---|---|
| free AbGUS | 2.079 ± 0.226 | 2.453 ± 0.171 | 8.361 ± 0.052 | 3.408 |
| $He_3Of_4$@UiO66@A | 1.8023 ± 0.136 | 3.147 ± 0.149 | 6.209 ± 0.072 | 1.972 |

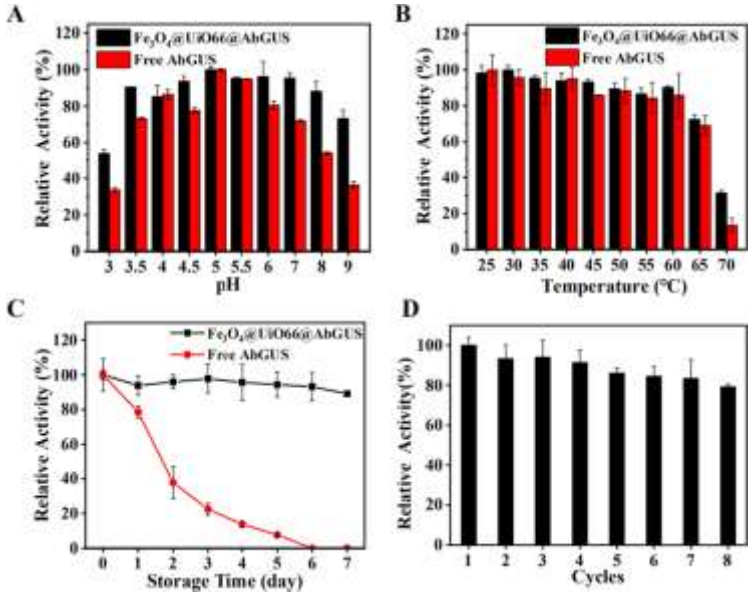


Rice. 6. Evaluation of the stability of immobilized enzymes under various conditions: stability after incubation for 2 hours in the pH range from 3.0 to 9.0 (A) and temperature from 25 to 70 ° C (B). (C) Long-term storage stability at 4°C in PB (pH 5.0, 20 mM) for 7 days. (D) Relative activity at pH 8.0 and 9.0, respectively. Thus, the immobilized enzymes showed a wide range of pH stability. The formation of coordination bonds between the unsaturated zirconium ion in the carrier and the undivided electron pair N on the histidine ring of the his-labeled protein [48] can increase the stiffness of enzymes and prevent the destruction of the tertiary structure of AbGUS. in alkaline media. Thus, the excellent alkaline stability of Fe Fe $_3$ O $_4$ @ UiO66 @ AbGUS markedly expanded the range of enzyme resistance to alkalis, which led to an expansion of its practical application, especially in high pH conditions. 6 B).

Long-term storage and reuse of immobilized enzymes are important for

industrial biocatalysis. As shown on Figure 6C, $Fe_3O_4$@UiO66@AbGUS almost saved 90% its catalytic activity, while free AbGUS completely lost its activity when stored for the same time. For resistance to protease degradation, residual activity its catalytic activity, while free AbGUS completely lost its activity when stored for the same time. For resistance to protease degradation, residual activity immobilized enzymes were 50% higher than the activity of free enzymes (rice. S5). Due to the presence of a porous structure in UiO66 MOF, the enzymes diffusing into the channel were to a certain extent UiO66@AbGUS under the same reaction conditions (pic.6D). The magnetic nanoparticles can be conveniently assembled by an external magnet after the reaction and re-dispersed by simple shaking. Residual activity of $Fe_3O_4$@UiO66@AbGUS decreased by only ~20% after eight cycles. The method of coordination connections made it difficult for the protein to fall away from the carriers.

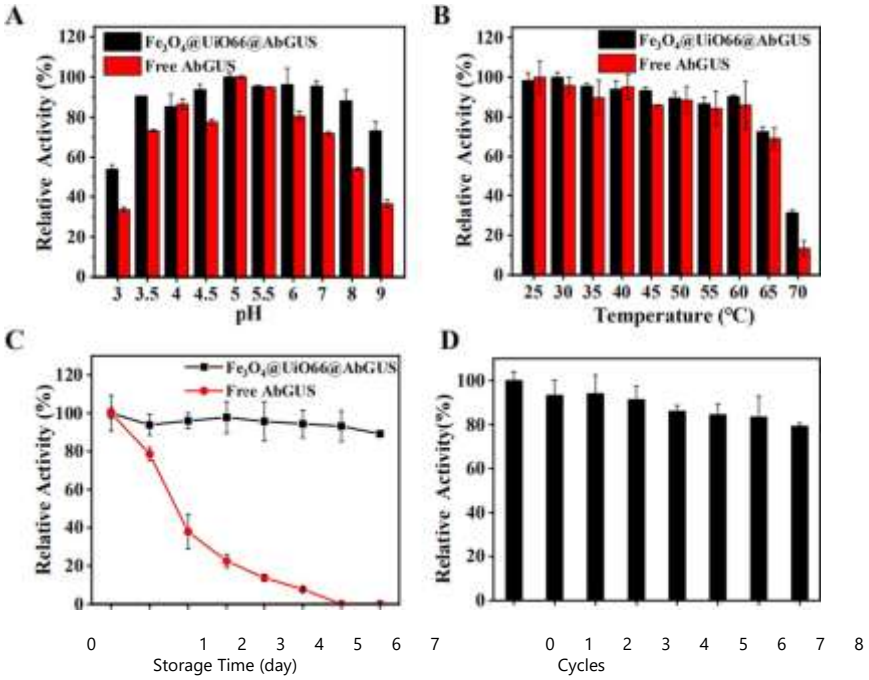


**Resistance to substrate and by-products and easy regeneration of $Fe_3O_4$ @UiO66@AbGUS.**

In the process of bioconversion, the accumulation of by-products often leads to inhibition of catalytic activity. Excessive accumulation of glucuronic acid probably inhibits the enzymatic activity of the model enzyme in this experiment and reduces the pH of the reaction system. The inhibitory effect of various concentrations of glucuronic acid on the activity of the enzyme was investigated. With 2 mM glucuronic acid, the catalytic activity of free AbGUS decreased by more than 50%, while the activity of immobilized enzymes was maintained at 92.8% ( Fig. 2). S7 ). Even when the concentration of glucuronic acid reached 8 mm, the residual activity of $Fe_3O_4$@UiO66@ AbGUS was more than twice the activity of free enzymes. The structure of the MOF can to a certain extent stabilize the conformation of enzymes, thereby ensuring that AbGUS can still have high catalytic activity at a higher concentration of the by-product.

To reduce the inhibitory effect of the byproduct on the activity of immobilized enzymes, we investigated the efficacy of $Fe_3O_4$@UiO66@AbGUS in the periodic reaction. The immobilized enzymes (0.5 mg) were first mixed with 2 mg/mL GL (2 mL, pH 5.0, 20 mM PB) and reacted at the optimum temperature.

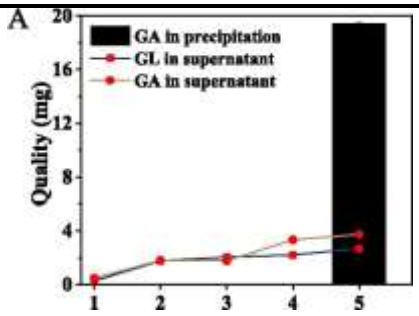


**Reaction Times**

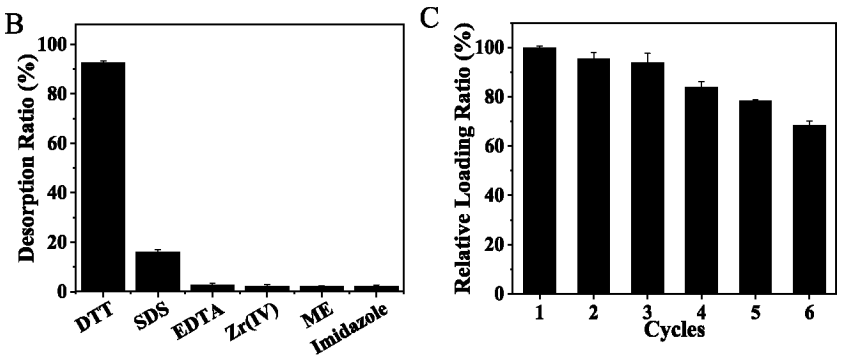


Figure 7. Application of immobilized enzymes and repair of carriers: (A) periodic hydrolysis of GL with recharge. (B) Desorption of immobilized enzymes by various reactants. (C) Recirculation of Fe3O4@UiO66 after treatment with dithiotreite (DTT) at high temperatures.

conditions. After collecting the magnetic composites, the supernatant was removed and a fresh GL solution of the same concentration was added again. The catalytic activity of $Fe_3O_4$@UiO66@AbGUS still retained 54.9% of the baseline activity after five loads (Figure 7A ). The amount of GA extracted from the precipitator was 59.8% of the theoretical yield, and 34.7% ga was collected from the supernatant by centrifugation. Thus, the magnetic carriers of the MOF provide efficient separation of substrate and product in the extraction of enzymes. This provided a good separation strategy for other heterogeneous biotransformation processes.

However, if not handled properly, heavy metals and organic ligands, as the primary synthetic MOF units, can cause new and serious environmental pollution problems. Thus, how effectively to reuse and regenerate a failed carrier has been identified as a hotspot of research in this area. [13,21] Enzymes immobilized by chemical covalent binding could be reusable, but this type of carrier often could not be reused. AbGUS self-organizes on the surface of $Fe_3O_4$@UiO66 due to the coordination interaction of oligohistidine labeled with $Zr^{4+}$ ions. We tested six types of regeneration reagents (Fig. 7B), such as imidazole (0.3 M), zirconium ion (0.3 M), mercaptoethanol (ME) (10%), ethylenediaminetetraacetic acid (EDTA) (0.3 M), DSN (10%), and DTT (5 mg/ml) to remove immobilized protein. However, none of the reactants were able to desorb the enzymes. Interestingly, after heating to 100° C. for 30 min, 92.6% of the absorbed protein was eluted at 5 mg/ml of DTT, while other chemicals remained at a very low level (less than 20%). As a reducing agent, DTT can restore protein disulfide bonds, which destroys the secondary structure of the protein. High temperatures revealed the tertiary structure of the protein and exposed the disulfide bonds in the protein that satisfy the working condition of DTT, which led to the desorption of the protein from $Fe_3O_4$@UiO66. 49 With an increase in DTT from 0 to 5 mg / ml ( Fig. S8 ) protein elutation rate increased significantly from 0 to 92%. With protein denaturation at high temperatures, a small amount of DTT could effectively desorb the protein from the carrier. After DTT treatment at high temperature, the immobilization of the protein on the magnetic carrier was maintained by more than 90% in the first three times of reuse and could still reach 70% after six times reuse (Figure 7C). Thus, the prepared

nanocarriers showed excellent recycling properties, which significantly reduced the cost and pollution of the environment.

## 2. Findings

This paper is the first to investigate zirconium-based magnetic MOFs ($Fe_3O_4$@UiO66) with highly selective immobilization and excellent renewability. Prepared MOFs demonstrated good magnetic response and relatively correct porous morphology, as well as specially captured His-labeled enzymes from cellular lysate. In addition, the immobilized enzymes had a wider range of pH and temperature, exhibiting more than 85% of the original activity after Premises on Wednesday with a pH of 3.5–8.0 or at 60 ° C for 2 h. The activity of immobilized enzymes was more than 80% after eight cycles. In addition, renewable magnetic carriers can effectively trap target proteins even after six times reuse. The above results suggest that the Zr(lV)-based magnetic MOF nanocarriers produced in this experiment can be used as a potential platform for one-step purification and immobilization of His-labeled enzymes. In addition, the excellent stability, reusability and renewability of the engineered nanoparticles have opened up very promising prospects for enzyme engineering and industrial catalysis.

## References


1. Lee, V. N.; Fan D.D. Biocatalytic strategies for the production of ginsenosides using g-glycosidase: current status and prospects. *Stated. microbiol. Biotechnologist.* 2020, *104,* 3807—3823.
2. Cheng, L.; Zhang, H.; Liang, X.; Sun, X.; Shen, X.; Wang, J.; Van, V.; Yuan, Q.; Rea, H.-I.; Kim, T.-M.; Kang, M.-S.; Linhardt, R. Enzymatic bioconversion of cycloastraghenol-6-O-^-D-glucoside in Cycloastraghenol using a novel recombinant b-glucosidase from Fizicocc sp. Soil748. *Process biochem.* 2019, 90, 81—88.
3. Q, L., Jr.; Tolman, V. B. Biologically inspired oxidation catalysis. *Nature* 2008, *455,* 333–340.
4. Kirk, O.; Borchert, TV; Fuglsang, CC Industrial Enzyme Applications. *Course. opinion Biotechnologist.* 2002, *13,* 345—351.
5. Shea, J.; Wu, Y.; Zhang, S.; Tian, Y.; Jan, D.; Jiang, Z. Bioinspired construction of multi-enzyme catalytic systems. *chem. soc.* 2018, *47, 4295—4313* .
6. Monajati, M.; Borande, S.; Hesami, A.; Mansouri, D.; Tamaddon, AM Immobilization of L-asparaginase on aspartic acid nanolist functionalized graphene oxide: enzyme kinetics and stability studies. *Chem. Eng. J. S. Smith.* 2018, *354,* 1153—1163.
7. Feng, X.; Liu, H.; Jia, J.; Chen, X.; Jiang, T.; Lee, K. Increasing the thermal stability of B-glucuronidase T. pinophilus allows biotransformation of glycyrrhizin at elevated temperatures. *chem. eng. nauch.* 2019, *204,* 91—98.
8. Altinkainak, K.; Tavlasoglu S.; Izdemir, N.; Osoy, I. A new generational approach to the immobilization of enzymes: organo-inorganic hybrid nanoflowers with increased catalytic activity and stability. *Enzyme microbe. Technol.* 2016, *93—94,* 105—112.
9. Franssen, MCR; Steunenberg, P.; Scott, E.L.; Zuilhof, X.; Sanders, JPM Immobilized enzymes in the production of biorecoverable energy sources. *chem. soc.* 2013, *42, 6491—6533* .
10. Zhang, S.; Lee, X.; Yuan, Q.; Secundo, F.; Lee, Yu.; Liang, H. Step-by-step immobilization of multi-enzymes using a zirconium-based coordination polymer, self-assembly in situ and specific absorption. *J. Neorg. Biochem.* 2020, 208, № 111093.
11. Alshawafi, VM; Aldhari, M.; Almulayki, YQ; Salah, N.; Moseli, SS; Ibrahim, I. Kh.; El-Shishtawi, RM; Mohamed, S.A. Immobilization of horseradish peroxidase on PMMA nanofibers is included with nanodiamond. *Artif. Cells Nanomed. Biotechnologist.* 2018, *46,* S973—S981.
12. Abdel-Magid, H.M.; El Leiti, H.M.; Mahran, LG; Fahmy, AS; Mader, K.; Mohamed, SA Development of a new flexible sugar

essential vesicles as carrier systems of the antioxidant enzyme catalase for application for wound healing. *Process biochem.* 2012, *47,* 1155—1162.

13. Liana, X.; Fang, Yu.; Joseph, E.; Wang, Q; Lee, J.; Banerjee, S.; Lollar, C.; Van, X.; Zhou, H.-K. Enzyme-MOF (organometallic framework) composites. *chem. soc.* 2017, *46, 3386—3401* .
14. Chong, G.-Y.; Ricco, R.; Liang, K.; Ludwig, J.; Kim, J.-O.; Falcaro, P.; Kim, D.-P. Bioactive scaffold MIL-88A hollow Spheres through interphase reaction Microfluidics inside the droplet for enzyme and encapsulation of nanoparticles. *chem. Mater.* 2015, *27,* 7903—7909.
15. Liang, K.; Ricco, R.; Doherty, cm; Styles, MJ; Bell, S.; Kirby, N.; Moody, S.; Haylock, D.; Hill, AJ; Dunan, CJ; Falcaro, P. Biomimetic mineralization of organometallic frameworks as Protective coatings for biomacromolecules. *National commune.* 2015, 6, № 7240.
16. Belluschi, M.; Guglielmi, P.; Masi, A.; Padella, F.; Singh, G.; Ya'qub, N.; Peddis, D.; Secchi, D. Magnetic metal is an organic frame composite using a quick and easy mechanochemical process. *neorg. chem.* 2018, 57, 1806—1814.
17. He, J.; Sun, S.; Zhou, Z.; Yuan, Q.; Liu, Y.; Liang, H. Thermostable immobilized enzyme, nickel-based magnetosensitive, organometallic framework nanorods as recyclable biocatalysts for efficient biosynthesis of S-adenosylmethionine. Dalton Trans. 2019, 48, 2077–2085.
18. Bell, DJ; Wiese, M.; Schoenberger, A.A.; Wessling M. Catalytically active membranes of hollow fibers with enzymes. Built-in organometallic framework coating. Angyu. chem., intl. Ed. 2020, 59, 16047-16053.
19. Application of magnetic composites m Ricco, R.; Malfatti, L.; Takahashi, M.; Hill, AJ; Falcaro, P. Application of magnetic composites metal-organic framework. J. Mater. chem. A 2013, 1, 13033. metal-organic frame. J. Mather. Chem. A 2013, 1, 13033.
20. Otari, SV; Patel, SCS; Potassium, VK; Lee, J. S. K. One step hydrothermal synthesis of magnetic rice straw to produce effective lipase immobilization and its application in esterification reaction. *Bioresource. Technol.* 2020, 302, № 122887.
21. Otari, SV; Patel, SCS; Potassium, VK; Lee, J. S. K. One step hydrothermal synthesis of magnetic rice straw to produce effective lipase immobilization and its application in esterification reaction. *Bioresource. Technol.* 2020, 302, № 122887.
22. Liang, S.; Wu, H.-L.; Xiong, J.; Tsung, M.-H.; Lou, V.-Yu. Metal-organic scaffolds as new matrices for efficient enzyme immobilization: an overview of updates. *Kordin. chem.* 2020, 406, № 213149 .
23. Wu, XL; Yue, X.; Zhang, Yu.Y.; Gao, XY; Lee, XY; Van, L.S.; Cao, Y. F.; Howe, M.; AN, NH; Zhang, L.; Lee, S.; Ma, JY; Lin, X.; Fu, Y.A.; Gu, Hong Kong; Lou, Wyoming; Wei, V.; Zare, R.N.; Ge, J. Packaging and delivery of enzymes using amorphous organometallic compounds. frames. *National commune.* 2019, 10, № 5165.
24. Knedel, T.-O.; Ricklefs, E.; Gatewayer, K.; Urlacher, V.B.; Janiak. Christoph, Encapsulation of laccase in the ZIF-8 Metal-Organic Framework demonstrates increased stability and substrate selectivity. *ChemistryOpen* 2019, 8, 1337-1344.
25. Liang, V.; Xu, H.; Carraro, F.; Maddigan, North Carolina; Lee, V.; Bell, S.G.; Huang, DM; Tarsia, A.; Solomon, MB; Amenich, H.; Vakkari, L.; Sumby, CJ; Falcaro, P.; Doonan, CJ Enhanced Activit y enzymes encapsulated in a hydrophilic organometallic framework. *Jam. chem. sots.* 2019, 141, 2348-2355.
26. Huang, V.-K.; Van, V.; Xue, K.; Mao, X. Effective Enzyme Immobilization on Magnetic Chitin Nanofiber Composite. *ACS Sustainable Chemical.* 2018, 6, 8118-8124.
27. He, LZ; Jan, YUS; Kim, J.; Yao, L.; Dong,

XW; Lee, th; Piao, YX Multilayer enzyme coating on highly conductive magnetic biochar nanoparticles for the detection of bisphenol A in water. *chem. eng. j.* 2020, *384,* № 123276.

28. Zhang, T.; Huang, British Columbia; Alsatari, AA; Alhamdi, A.; Yue, W.; Dan, Y. H. Synthesis of pod-shaped magnetic mesoporous silica Nanocycles for use as support enzymes and nanomechanters in biocatalysis. ACS *Mater App. Interfaces* 2020, *12,* 17901-17908.
29. Veldemgret, T.G.; Nisola, Grandmaster; Ramos, CMP; Banares, AB; Valdehueza, KNG; Lee, V.K.; Chang, WJ Tyrosinase-Catalyzed phenol-mediated immobilization of beta-agarase to L-coated magnetic particles for the production of neo-agarooligosa ccharides from Gelidium amansii. *ACS Sustainable Chemical.* 2020, *8* , 3573-3582.
30. Zhang, Yu.; Jan, Y.; Ma, V.; Go, J.; Lin, Y.; Wang, K. Uniform Microspheres with magnetic core/shell, functionalized $Ni^{2+}$ -iminody- acetic acid for single-stage purification and immobilization of its labeled enzymes. ACS *Mater. Interfaces* 2013, 5, 2626-2633.
31. Roder, R.; Preifi, T.; Hirschl, P.; Steinborn, B.; Zimpel, A .; Hon, M.; Radler, J. S. A.; Bain, T.; Wagner, E.; Wuttke, S.; Lachelt, U. Multifunctional nanoparticles by coordinating self-assembly of it- Labeled blocks with organometallic frames. *Jam. chem. sots.* 2017, *139,* 2359-2368.
32. Orkahada, P.; Gref R.; Baati, T.; Allan, PC; Maureen, G.; Couvreur, P.; Ferey, G.; Morris, RE.; Serr, K. Metal-organic Frames in biomedicine. *chem. 2012, 112,* 1232.
33. Porat, J. Affinity chromatography with immobilized metal ions. *Purif protein expression.* 1992, 3, 263-281.
34. Liu, CX; Yuan, J. L.; Gao, H.F.; Liu, CQ Biodiesel production from waste vegetable oil immobilized lipase on superparamagnetic hollow submicrospheres Fe3O4. *Biocatal Biotrans form.* 2016, 34, 283-290.
35. Qi, BK; Luo, JQ; Wan, YH Immobilization of cellulase into organometallic framework composites with a core-shell structure: better resistance to inhibitors and easier disposal. *Bioresource. Technol.* 2018, 268, 577-582.
36. Farh, HS; Hasanzade, M.; Nashtai, M.S.; Rabbani, M.; Haji, A.; Hadawi Moghadam, B. IPP-dendrimer-functionalized magnetic Organometallic framework (Fe3O4@ MOF @PPl) with high adsorption capacity for sustainable wastewater treatment. *ACS Mather. Interfaces* 2020, *12,* 25294-Liang, S.; Wu, H.-L.; Xiong, J.; Zong, M.-H.; Lu, W.-Y. Metal-organic scaffolds as new matrices for efficient enzyme immobilization: an overview of updates. *Kordin. chem.* 2020, 406, № 213149.
37. Wu, XL; Yue, X.; Zhang, Yu.Y.; Gao, XY; Lee, XY; Van, L.S.; Cao, Y. F.; Howe, M.; AN, NH; Zhang, L.; Lee, S.; Ma, JY; Lin, X.; Fu, Y.A.; Gu, Hong Kong; Lou, Wyoming; Wei, V.; Zare, R.N.; Ge, J. Packaging and delivery of enzymes using amorphous organometallic compounds. frames. *National commune.* 2019, 10, № 5165.
38. Knedel, T.-O.; Ricklefs, E.; Gatewayer, K.; Urlacher, V.B.; Janiak. Christoph, Encapsulation of laccase in the ZIF-8 Metal-Organic Framework demonstrates increased stability and substrate selectivity. *ChemistryOpen* 2019, 8, 1337-1344.
39. Liang, V.; Xu, H.; Carraro, F.; Maddigan, North Carolina; Lee, V.; Bell, S.G.; Huang, DM; Tarsia, A.; Solomon, MB; Amenich, H.; Vakkari, L.; Sumby, CJ; Falcaro, P.; Doonan, CJ Enhanced Activit y enzymes encapsulated in a hydrophilic organometallic framework. *Jam. chem. sots.* 2019, 141, 2348-2355.
40. Huang, V.-K.; Van, V.; Xue, K.; Mao, X. Effective Enzyme Immobilization on Magnetic Chitin Nanofiber Composite. *ACS Sustainable Chemical.* 2018, 6, 8118-8124.
41. He, LZ; Jan, YUS; Kim, J.; Yao, L.; Dong, XW; Lee, th; Piao, YX Multilayer enzyme coating on highly conductive magnetic

biochar nanoparticles for the detection of bisphenol A in water. *chem. eng. j.* 2020, *384,* № 123276.

42. Zhang, T.; Huang, British Columbia; Alsatari, AA; Alhamdi, A.; Yue, W.; Dan, Y. H. Synthesis of pod-shaped magnetic mesoporous silica Nanocycles for use as support enzymes and nanomechanters in biocatalysis. ACS *Mater App. Interfaces* 2020, *12,* 17901-17908.
43. Veldemgret, T.G.; Nisola, Grandmaster; Ramos, CMP; Banares, AB; Valdehueza, KNG; Lee, V.K.; Chang, WJ Tyrosinase-Catalyzed phenol-mediated immobilization of beta-agarase to L-coated magnetic particles for the production of neo-agarooligosa ccharides from Gelidium amansii. *ACS Sustainable Chemical.* 2020, *8* , 3573-3582.
44. Zhang, Yu.; Jan, Y.; Ma, V.; Go, J.; Lin, Y.; Wang, K. Uniform Microspheres with magnetic core/shell, functionalized $Ni^{2+}$ -iminody- acetic acid for single-stage purification and immobilization of its labeled enzymes. ACS *Mater. Interfaces* 2013, 5, 2626-2633.
45. Roder, R.; Preifi, T.; Hirschl, P.; Steinborn, B.; Zimpel, A .; Hon, M.; Radler, J. S. A.; Bain, T.; Wagner, E.; Wuttke, S.; Lachelt, U. Multifunctional nanoparticles by coordinating self-assembly of it- Labeled blocks with organometallic frames. *Jam. chem. sots.* 2017, *139,* 2359-2368.
46. Orkahada, P.; Gref R.; Baati, T.; Allan, PC; Maureen, G.; Couvreur, P.; Ferey, G.; Morris, RE.; Serr, K. Metal-organic Frames in biomedicine. *chem. 2012, 112,* 1232.
47. Porat, J. Affinity chromatography with immobilized metal ions. *Purif protein expression.* 1992, 3, 263-281.
48. Liu, CX; Yuan, J. L.; Gao, H.F.; Liu, CQ Biodiesel production from waste vegetable oil immobilized lipase on superparamagnetic hollow submicrospheres Fe3O4. *Biocatal Biotrans form.* 2016, 34, 283-290.
49. Qi, BK; Luo, JQ; Wan, YH Immobilization of cellulase into organometallic framework composites with a core-shell structure: better resistance to inhibitors and easier disposal. *Bioresource. Technol.* 2018, 268, 577-582.
50. Farh, HS; Hasanzade, M.; Nashtai, M.S.; Rabbani, M.; Haji, A.; Hadavi Moghadam, B. IPP-dendrimer-functionalized magnetic Organometallic framework ($Fe_3O_4$@ MOF@PPl) with high adsorption capacity for sustainable wastewater treatment. *ACS Mater App. Interfaces* 2020, *12,* 25294-25303.
51. Chen, R.; Tao, K.-A.; Zhang, Z.; Chen, X.; Liu, Z.; Wang, J . Layer-by-layer manufacture of the core-shell Fe3O4@UiO-66-NHc.
52. Ho, J.-B.; Xu, L.; Chen, X.; Zhang, Yu.; Ian, J.-C.E.; Yuan, B.; Fu, M.-L. Direct epitaxial synthesis of magnetic Fe3O4@UiO-66 composite for effective removal of arsenate from water. *Microporous mesoporous matter.* 2019, 276, 68-75.
53. Wu, M.-H.; Gao, J.; Wang, F.; Jan, J.; Pesnya, N .; Gene, X.; Mi, P.; Tian, J.; Luo, J.; Liang, F.; Yan, Y.-V. Multistimules Responsive Core-Shell Nanoplatform built of Fe3O4@MOF with Pillar[6]aren nanons. *Maly* 2018, 14, No 1704440.
54. Chao, K.; Liu, J.; Wang, J.; Zhang, Yu.; Zhang, B.; Zhang, Yu.; Xiang, X.; Chen R. Modification of the surface of galluasite nanotubes with dopamine for the immobilization of enzymes. *ACS Mater. Interfaces* 2013, 5, 10559-10564.
55. Torabizadeh, Kh.; Mahmoudi, A. Hydrolysis inulina inulinase. covalently immobilized on magnetic nanoparticles prepared with wheat gluten hydrolysates. *Biotechnologist.* 2018, *17,* 97-103 .
56. Das, R.; Talat, M.; Srivastava, Ontario; Kayastha, AM
57. Covalent immobilization of peanut amylases to produce industrial nanobiocatalysts: a comparative study of the kinetics, stability and reuseability of an immobilized enzyme. *Food chemistry.* 2018, *245,* 488-499.
58. Kadam, A.A.; Jang, J.; Gee, South Carolina; Sun, J.-S.; Lee, D.S. Supermagnetic

galluasite nanotubes, functionalized with chitosan, for covalent immobilization of laccase. *carbohydrate. Poly m.* 2018, *194,* 208 216.

59. Nadar, SS; Varadan, NO; Suresh, S.; Rao, P.; Ahirrao, DJ; Adsar, S. Recent progress in the field of nanostructured magnetic framework. composites (MFC): synthesis and application. *J. Taiwan Inst. chem. eng.* 2018, *91,* 653-677.
60. Jannakopoulo, A.; Gkantsu, E.; Polydera, A.; Stamatis, H. Multi-enzyme nanoassembly: recent advances and applications. *Biotechnology trends.* 2020, 38, 202-216.
61. Mehta, J.; Bhardwaj, N.; Bhardwaj, SC; Kim, K.-H.; Dip, A. Recent advances in methods of enzyme immobilization: organometallic frameworks as new substrates. *Coordinated Chemistry 2016*, 322, 30-40.
62. Ge, M.; Zhang, J.; Guy, Z.; Fan, R.; Hu, S.; Liu, G.; Cao, Y.; Doo, H.; Shen Y. Synthesis of magnetic Fe3O4@PS-ANTA-M2+ (M = Ni, Co, Cu and Zn) of the nanosphere for the specific isolation of histidine-labeled proteins. *chem. eng. j.* 2021, 404, № 126427.
63. Doperalsky, P.; Michoff, MEZ; Marx, D. Mechanochemical disulfide reduction reveals imprints of a non-covalent sulfur-oxygen chalcogen bond in protein-inspired mimetics in an aqueous solution. *phys. chem. chem. phys.* 2020, 22, 25112-25117.